MATHEMATICAL MODELING OF LASER ABLATION IN LIQUIDS WITH APPLICATION TO LASER ULTRASONICS

R. J. Conant and S. E. Garwick
Department of Mechanical and Industrial Engineering
Montana State University
Bozeman, MT 59717

INTRODUCTION

The use of pulsed lasers to produce ultrasonic waves in materials has proven to be attractive in many applications. However, one of the limitations of laser ultrasonics is the weak signal strength produced by thermoelastic sources. One way to improve signal strength is to use laser intensities that are high enough to ablate the material surface. While ablation leads to surface damage in solids, it is generally not a problem in liquids. Consequently ablation is a viable means of enhancing signal strength for laser ultrasonics applications such as high temperature materials processing involving molten metals. Experiments carried out at the Idaho National Engineering Laboratory (INEL) on liquid mercury, using the experimental setup shown in Fig. 1a, indicate that the signal strength can be increased two orders of magnitude through ablation [1]. Mercury is a nearly ideal material with which to study ablation in molten metals because it is liquid at room temperature and its properties are well known. The results of the experiments carried out at the INEL are shown in Fig. 1b. For laser intensities below about 6 MW/cm^2 the ultrasonic signal results from thermoelastic sources (rapid thermal expansion) while at intensities above about 20 MW/cm^2 ablation is the dominant mechanism A transition between rapid thermal expansion and ablation occurs between 6 MW/cm^2 and 20 MW/cm^2.

During ablation, vapor molecules are ejected from the liquid surface. The recoil momentum of these ejected molecules results in a pressure on the surface which causes an acoustic wave to propagate through the liquid. This paper describes a mathematical model for predicting the pressure distribution caused by ablation.

Laser ablation has been studied by several researchers. Interest has generally focused on understanding the gas dynamics of ablation and on the use of laser ablation in drilling processes. Papers most pertinent to the current work, and which contain additional references, are those of Anisimov [2], Anisimov and Rakhmatulina [3], Knight [4, 5], and Zweig [6]. Each of these works is based on a one-dimensional steady state model in which the vapor phase is treated as an ideal gas, an approach that is adopted in the present work.

Review of Progress in Quantitative Nondestructive Evaluation, Vol 16
Edited by D.O. Thompson and D.E. Chimenti, Plenum Press, New York, 1997

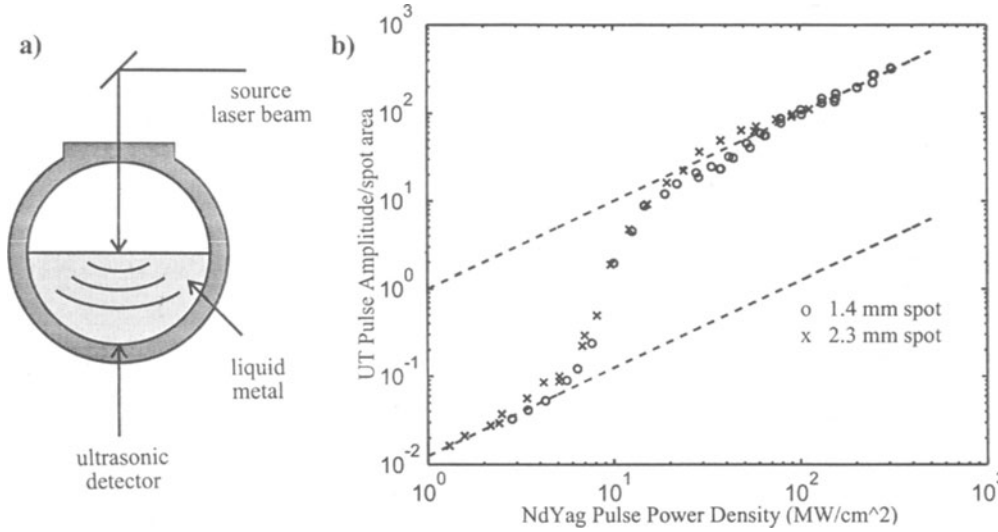

Figure 1. a). Experimental setup for measuring ultrasonic amplitude. b). Experimental results.

MATHEMATICAL FORMULATION

General

A portion, I_{therm}, of the absorbed power density, I_{abs}, is required to raise the liquid to the saturation temperature and the remainder, I_{evap}, causes vaporization. Thus,

$$I_{abs} = I_{therm} + I_{evap} . \tag{1}$$

The output power density of the laser is given by

$$I_{laser} = \frac{I_{abs}}{1 - R} + I_{loss} \tag{2}$$

where R is the surface reflectance of the liquid and I_{loss} is the power density lost between the laser source and the surface of the liquid. These losses occur, for example, because of scattering as the laser light passes through the glass and, as vaporization is occurring, as it passes through the vapor.

Figure 2a shows the flow regions included in the model and Fig. 2b the corresponding x-t diagram. Rapid deposition of laser energy onto the liquid surface raises the surface temperature to the saturation temperature, T_s, at which point vaporization begins. At the laser intensities of interest, the evaporation rate is large and the vapor near the surface is not in translational equilibrium because of the random motion of the molecules However, translational equilibrium is attained within a few atomic mean free paths of the surface and the usual equations of gas dynamics apply. The region where translational equilibrium does not exist, referred to as a Knudsen layer, moves with the liquid surface and is very thin.

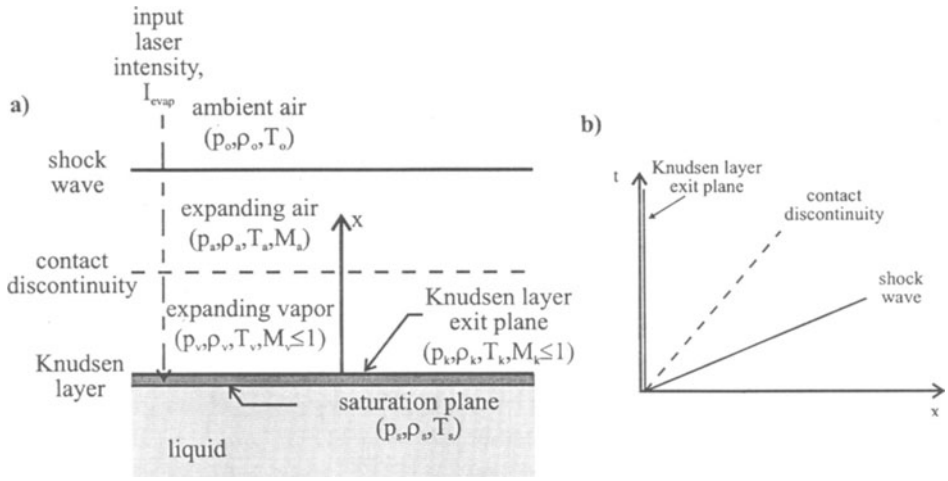

Figure 2. a). Flow regions for subsonic model. b). x-t diagram for subsonic model.

From the point of view of gas dynamics it is treated as a discontinuity surface across which jumps in absolute temperature, T, and density, ρ, are calculated as [5],

$$r_T = \frac{T_K}{T_s} = \left[\sqrt{1 + \pi \left(\frac{\gamma_v - 1}{\gamma_v + 1} \frac{m}{2} \right)^2} - \sqrt{\pi} \frac{\gamma_v - 1}{\gamma_v + 1} \frac{m}{2} \right]^2 \tag{3}$$

$$r_\rho = \frac{\rho_K}{\rho_s} = \sqrt{\frac{1}{r_T}} \left[\left(m^2 + \frac{1}{2} \right) \exp(m^2)\, erfc(m) - \frac{m}{\sqrt{\pi}} \right] + \frac{1}{2} \frac{1}{r_T} \left[1 - \sqrt{\pi}\, m \exp(m^2)\, erfc(m) \right] \tag{4}$$

where the subscript *s* refers to the saturation plane, *K* refers to the Knudsen layer exit plane, and *v* refers to the fluid in the vapor phase. γ is the ratio of specific heats (assumed constant for a given phase), *erfc* is the complementary error function, and

$$m = \sqrt{\frac{\gamma_v}{2}} M_K . \tag{5}$$

In Eq. (5), M = *u* / *a* is the Mach number. *u* is the fluid velocity and *a* is the local sound speed.

The pressure on the liquid surface is found by considering a control volume that straddles the liquid surface and the Knudsen layer, and moves with the liquid surface. Conservation of momentum then gives

$$p_\ell = p_K(1 + \gamma_v M_K^2) \tag{6}$$

where p is the absolute pressure, the subscript ℓ refers to the fluid in the liquid phase, and the momentum of the liquid relative to the control volume has been ignored since, typically, $\rho_K/\rho_\ell << 1$.

The sudden deposition of energy causes a shock wave to propagate away from the surface. A contact discontinuity separates the compressed air behind the shock wave from the expanding vapor. Across the contact discontinuity, the normal component of velocity is continuous, as is the pressure. The velocity of the air behind the shock front is given by a Rankine-Hugoniot relation (see, for example, [7]). When the continuity conditions across the contact discontinuity are used, the resulting expression divided by the local sound speed in the vapor, $a_v = \sqrt{\gamma_v \Re_v T_v}$ where $\Re$ is the gas constant, and the ideal gas law used, the following expression results, after some rearrangement, for the Mach number in the vapor

$$M_v = \frac{a_0 / \gamma_0}{\sqrt{\gamma_v \Re_v \frac{r_T}{R_T} T_s}} \frac{\frac{1}{p_0}\frac{r_\rho}{R_\rho}\frac{r_T}{R_T} p_s - 1}{\sqrt{1 + \frac{\gamma_0 + 1}{2\gamma_0}\left(\frac{1}{p_0}\frac{r_\rho}{R_\rho}\frac{r_T}{R_T} p_s - 1\right)}} \tag{7}$$

where the subscript *0* refers to the ambient air ahead of the shock and

$$R_\rho = \frac{\rho_K}{\rho_v}; \qquad R_T = \frac{T_K}{T_v}. \tag{8}$$

An energy balance applied to the control volume yields an equation that can be solved for ρ_K, the density at the Knudsen layer exit plane, in terms of I_{evap}. Equation (4) is then used to obtain ρ_s in terms of I_{evap} and the result substituted into the ideal gas law for the saturated vapor. This leads to an equation relating the saturation pressure to I_{evap}.

$$p_s = \frac{I_{evap}}{\gamma_v M_K H_{LV}} \frac{1}{r_\rho} \sqrt{\frac{1}{r_T}} \sqrt{\gamma_v \Re_v T_s} \tag{9}$$

where H_{LV} is defined as

$$H_{LV} = H_V - H_L + \frac{1}{2} M_K^2 a_K^2 \tag{10}$$

H_V and H_L are the specific enthalpies for the saturated vapor and saturated liquid, respectively, obtained from published saturation data for mercury [8].

Another expression for the saturation pressure is obtained by assuming that the relationship between the saturation pressure and the saturation temperature of the fluid can be adequately described by the Clausius-Clapeyron relation,

$$p_s = P^* \exp(-T^*/T_s) \tag{11}$$

where P^* and T^* are constants. Following Zweig [6], the values of these constants were found by fitting published saturation data for mercury [8] with Eq. (11). With values of $P^* = 5.846\times10^4$ atm, and $T^* = 6914.96$ °K, Eq. (11) predicts the saturation pressure values in [8] to within 1.2%

Subsonic Flow

For laser intensities low enough that $M_K < 1$, the state in the vapor region is uniform. Therefore

$$R_\rho = 1, \qquad R_T = 1, \qquad M_K = M_v. \tag{12}$$

With a given value of I_{evap} and prescribed ambient conditions, the equations (3), (4), (7), (9), and (11) then contain 5 unknown quantities: p_s, T_s, M_K, r_ρ, and r_T. Once these equations are solved, p_K can be obtained from

$$p_K = \frac{p_K}{p_s} p_s = r_\rho r_T p_s \tag{13}$$

and the interface pressure obtained from Eq. (6).

Supersonic Flow

As I_{evap} increases, the flow velocity at the exit plane of the Knudsen layer increases to Mach 1. Further increases in I_{evap} result in thermal choking of the flow. Thus the flow leaving the Knudsen layer can never exceed sonic velocity (see, for example, [9]) Downstream of the Knudsen layer, however, the streamlines diverge enabling the flow to accelerate to supersonic velocities. This acceleration takes place through a centered Q-rarefaction fan [10]. The flow regions for this situation are shown in Fig 3a and Fig. 3b shows the corresponding x-t diagram. Since the state of the fluid changes across the fan, Eqs. (12) are no longer valid. However, in a Q-rarefaction fan the Riemann invariant $P = u + 2a/(\gamma_v - 1)$ is constant and the flow is isentropic. P is evaluated at the exit of the rarefaction fan and equated to the value obtained at the Knudsen layer exit plane where $u_K = a_K$. Thus, across the fan,

$$\sqrt{R_T} = \frac{2}{\gamma_v + 1} + \frac{\gamma_v - 1}{\gamma_v + 1} M_v, \qquad R_T = R_\rho^{\gamma_v - 1}. \tag{14}$$

Equations (14), together with the condition that $M_K = 1$, provide the additional equations needed when I_{evap} is above the value required to produce sonic flow at the Knudsen layer exit plane.

Figure 4 shows the acoustic pressure, $p_\ell - p_0$, at the liquid surface as a function of I_{evap}.

Quasi-Two-Dimensional Formulation

For an illuminated spot of radius r_o and area A_{spot} the average acoustic pressure is

$$\langle p_{acoustic} \rangle = \frac{2\pi}{A_{spot}} \int_0^{r_o} [p(r) - p_0]\, r\, dr \qquad (15)$$

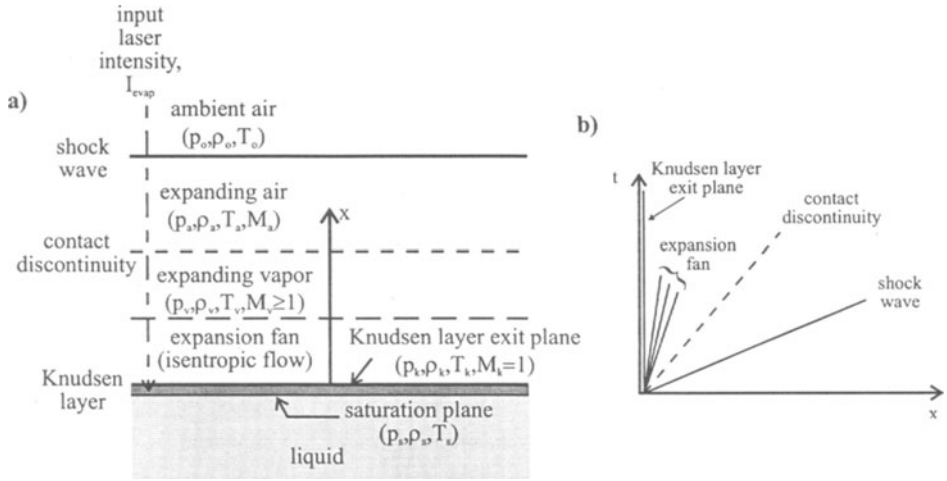

Figure 3. a). Flow regions for supersonic model. b). x-t diagram for supersonic model.

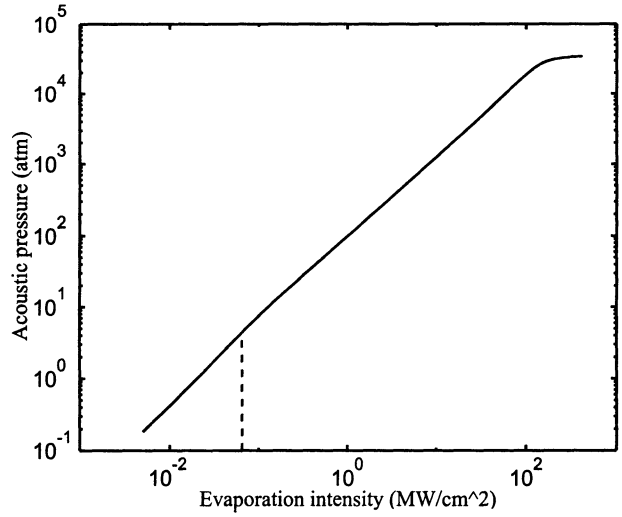

Figure 4. Acoustic pressure at the liquid surface vs. I_{evap}. The dashed line indicates the point at which $M_K = 1$.

where p(r) is the absolute pressure at the liquid surface. A quasi-two-dimensional formulation is obtained by replacing p(r) in Eq. (15) with p_ℓ obtained from Eq. (6). The radial dependence of the pressure follows indirectly from the fact that $p_\ell = p_\ell[I_{evap}(r)]$. It is assumed that the linear acoustic equations hold in the liquid so that the signal strength is proportional to $\langle p_{acoustic} \rangle$.

In Eq. (1), $I_{therm} \approx \rho_\ell \, \delta \, c \, (T_s - T_0) / t_p$ where δ is the optical penetration depth in the liquid, c is the specific heat of the liquid, and t_p is the laser pulse duration. T_s is taken to be the vaporization temperature at a pressure of one atmosphere.

Results are calculated for a laser intensity that is uniform over the illuminated spot, and for a Gaussian radial distribution. Figure 5 shows these results, with I_{loss} in Eq. (2) chosen as zero, along with the experimental results for mercury Note that on a log-log plot, the proportionality constant relating signal strength to <p> simply shifts the theoretical curves vertically. Since the value of the proportionality constant depends on, among other things, the details of the detector and its associated electronics, it is considered to be a free parameter and its value chosen such that the theoretical curves match the experimental data at high laser intensities. The theory predicts a linear relationship between laser intensity and signal strength at high laser intensities, in agreement with the experimental results. However, the theory predicts that the onset of ablation occurs at a lower laser intensity than shown in the experiments. This may be due to losses in laser intensity prior to the laser light reaching the surface of the mercury, and due to the calculation of I_{therm} in which the vaporization temperature at a saturation pressure of one atmosphere is used. In fact, the saturation temperature increases with increasing laser intensity. When the theoretical curves are translated along the upper dashed line of Fig. 5 until the intensity at which ablation begins agrees with that observed in the experimental results, as shown in Fig 6, the agreement between theory and experiment is very good.

CONCLUSIONS

A one-dimensional, steady state model of laser ablation has been developed to predict the pressure at the liquid surface. This has been used in a quasi-two-dimensional model to

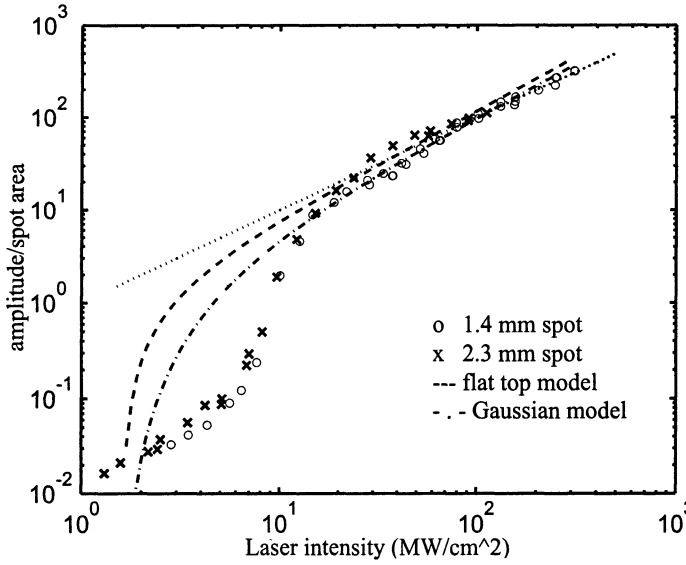

Figure 5. Comparison of model and experimental results for mercury.

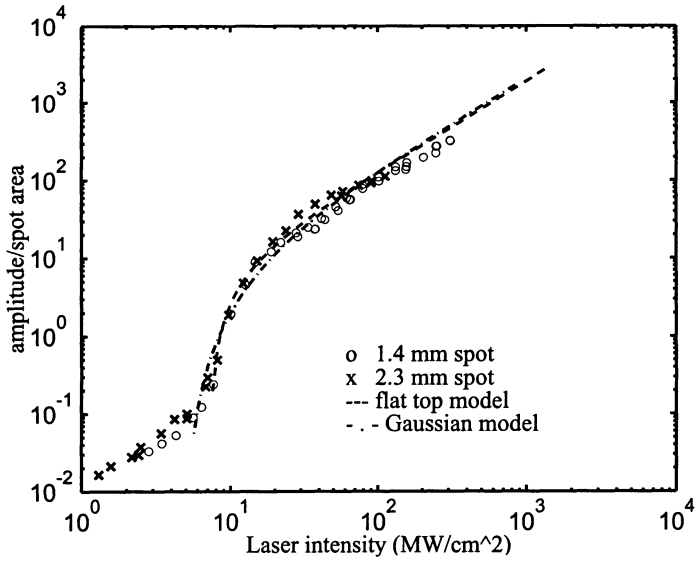

Figure 6. Model results shifted to match the onset of ablation seen in the experimental results.

give average pressure vs. laser intensity. Results predicted by the model for mercury are in general agreement with the results of experiments conducted at the INEL. At high laser intensities, the model predicts a linear relationship between pressure and intensity, in agreement with the experiments; in the region of transition from thermal expansion to ablation, the curve shape predicted by the model is in qualitative agreement with experimental results. The model predicts that the onset of ablation occurs at lower laser intensities than observed in the experiments, suggesting that losses are present that are not accounted for in the model.

ACKNOWLEDGMENTS

This work was supported in part by NSF EPSCoR under contract OSR93505-46. The authors thank K. L. Telschow and J. B. Walter for providing the experimental data and for several fruitful discussions during the course of the work.

REFERENCES

1. J. B. Walter, K. L. Telschow and R. J. Conant, in *Review of Progress in QNDE*, Vol. 14, eds. D. O. Thompson and D. E. Chimenti (Plenum, New York, 1995), p. 507.
2. S. I. Anisimov, Soviet Physics JETP 27, 182 (1968).
3. S. I. Anisimov and A. Kh. Rakhmatulina, Soviet Physics JETP 37, 441 (1974).
4. C. J. Knight, J. Fluid Mech. 75, 469 (1976).
5. C. J. Knight, AIAA Journal 17, 519 (1979).
6. A. D. Zweig, J. Appl. Phys. 70, 1684 (1991).
7. H. W. Liepman and A. Roshko, *Elements of Gas Dynamics*, (Wiley, New York, 1957), p. 64.
8. G. J. Van Wylen and R. E. Sonntag, *Fundamentals of Classical Thermodynamics*, 2nd ed. (Wiley, New York, 1978), p. 680.
9 A H. Shapiro, *The Dynamics and Thermodynamics of Compressible Fluid Flow*, (Ronald, New York, 1953), I, Chap. 7.
10. J. A. Owczarek, *Fundamentals of Gas Dynamics*, (International, Scranton, 1964), p. 315.